Geophysical Research Letters

RESEARCH LETTER
10.1029/2021GL095610

The Phase-Locking of Tropical North Atlantic and the Contribution of ENSO

Han-Ching Chen[1], **Fei-Fei Jin**[1], **and Leishan Jiang**[1]

[1]Department of Atmospheric Sciences, University of Hawai'i at Mānoa, Honolulu, HI, USA

Key Points:

- By considering the seasonal modulation of local feedbacks and remote ENSO forcing, the SDM model can well reproduce the TNA phase-locking
- In observations, the role of local TNA feedbacks and ENSO forcing are equivalently important in TNA phase-locking
- The TNA phase-locking strength associated with ENSO is highly correlated with the relationship between ENSO and TNA

Supporting Information:

Supporting Information may be found in the online version of this article.

Correspondence to:

H.-C. Chen and F.-F. Jin,
hanching@hawaii.edu;
jff@hawaii.edu

Citation:

Chen, H.-C., Jin, F.-F., & Jiang, L. (2021). The phase-locking of Tropical North Atlantic and the contribution of ENSO. *Geophysical Research Letters*, *48*, e2021GL095610. https://doi.org/10.1029/2021GL095610

Received 13 AUG 2021
Accepted 18 NOV 2021

Abstract The Tropical North Atlantic (TNA) is characterized by significant interannual variability in sea surface temperature (SST), which is phase-locked to the boreal spring. In this study, the phase-locking of TNA is investigated by adopting a linear stochastic-dynamical model (SDM) using seasonally modulated TNA feedbacks together with the seasonal modulation of ENSO forcing. In the observations, the role of local TNA feedbacks and ENSO forcing in TNA phase-locking are equivalently important with both preferring the peak of TNA variability to appear in the boreal spring. Besides, the seasonal modulation of TNA feedbacks and ENSO forcing strength are both mainly controlled by thermodynamic processes. In most climate models, the contribution of ENSO on TNA phase-locking is weaker than that in observations. The strength of ENSO-related TNA phase-locking is highly correlated with the relationship between ENSO and TNA, which is mainly determined by the amplitude of ENSO and its teleconnection patterns.

Plain Language Summary The interannual variability of sea surface temperature (SST) in the Tropical North Atlantic (TNA) is a prominent climate mode occurring in the Atlantic. TNA SST anomalies usually grow during boreal winter, reach their maximum amplitude in boreal spring and then decay in the summer and fall, called TNA phase-locking phenomenon. Although understanding the phase-locking of TNA is important for predicting the TNA and determining the global TNA teleconnection, there is very little discussion of the mechanisms of TNA phase-locking in the literature. In this study, we develop a conceptual stochastic-dynamical model (SDM) using seasonally modulated TNA feedbacks with seasonal modulation of ENSO forcing to investigate the features and mechanisms of TNA phase-locking. The SDM simulations can well reproduce the TNA phase-locking for observations and CMIP models. The mechanisms of TNA phase-locking and the contribution of ENSO on TNA phase-locking are discussed.

1. Introduction

The variability of sea surface temperature (SST) in the Tropical North Atlantic (TNA) is one of the dominant climate modes in the tropical Atlantic and plays a crucial role in global climate and weather. TNA SST anomalies (SSTAs) usually grow during boreal winter, reach their maximum amplitude in boreal spring and then decay in the summer and fall (Breugem et al., 2007; Chiang et al., 2002; Czaja et al., 2002); this is known as the TNA phase-locking phenomenon. Although understanding the phase-locking of TNA is important for predicting the TNA and determining the global TNA teleconnection, there is very little discussion in the literature on the mechanisms of TNA phase-locking. Breugem et al. (2007) attributed the TNA phase-locking to the seasonal migration of the climatological intertropical convergence zone (ITCZ). The local wind-evaporation-SST (WES) feedback is positive in boreal winter and spring due to the opposition of the anomalous and mean winds when the ITCZ is located near the equator, but the WES feedback is negative in summer and fall due to the same direction of the anomalous and mean winds when the ITCZ moves northward away from the equator.

In addition to the local thermodynamics adjustment of the atmosphere to TNA SSTA, the teleconnection of remote forcing, such as El Niño–Southern Oscillation (ENSO), can also have an impact on TNA SSTA (Alexander & Scott, 2002; Chiang & Sobel, 2002; Enfield & Mayer, 1997; Jiang & Li, 2019; Klein et al., 1999; Saravanan & Chang, 2000). TNA SSTA could be impacted by ENSO via two main mechanisms. One mechanism is through the ENSO-related low-level Pacific North American (PNA) pattern, where an anomalous low-pressure system located in the southeastern United States reduces the trade winds over the TNA region (Alexander & Scott, 2002; Enfield & Mayer, 1997; Giannini et al., 2000; Klein et al., 1999). Another way to affect TNA is through the ENSO-induced Gill response to suppress rainfall in the tropical Atlantic, which then generates an anomalous anticyclonic circulation to weaken the TNA trade winds (García-Serrano et al., 2017). Through these two mechanisms,

ENSO-induced changes in the strength of the trade winds lead to changes in wind-related surface latent cooling and generate anomalous SST a few months after ENSO's winter peak phase (Jiang & Li, 2019). Some studies (Chang et al., 2000; Czaja, 2004) suggest that the seasonal dependence of the remote forcing by ENSO could determine the seasonal variation of TNA SSTA.

The above studies proposed possible mechanisms to explain the phase-locking of TNA; however, a qualitative understanding of the relative contribution of phase-locking to the local TNA feedbacks and remote ENSO forcing is still elusive. Moreover, the ability of coupled ocean-atmosphere general circulation models (CGCMs) to capture TNA phase-locking remains inconclusive. In this study, we utilize a conceptual stochastic model framework to investigate the characteristics and mechanisms of TNA phase-locking in observations and compare it with CMIP5 and CMIP6 models. Here, we show that TNA phase-locking in observations and CMIP models can be well reproduced by the linear stochastic model framework, and in the observations, the role of local TNA feedbacks and ENSO forcing in TNA phase-locking are equivalently important. The contribution of ENSO forcing on TNA phase-locking in climate models is further discussed.

2. Data and Methods

2.1. Observations and CMIP Models

The observed SST used in this study is from the monthly Hadley Centre Global Sea Ice and Sea Surface Temperature data set (HadISST; Rayner et al., 2003). The 850 hPa wind, 850 hPa geopotential height, surface latent heat flux, surface sensible heat flux, surface shortwave radiation, and surface longwave radiation are from the fifth generation of ECMWF atmospheric reanalysis of the global climate (ERA5; Hersbach et al., 2020). The simulated outputs are taken from the Coupled Model Intercomparison Project Phase 5 (CMIP5; Taylor et al., 2012) and 6 (CMIP6; Eyring et al., 2016). Only the first ensemble member of the CMIP5 (r1i1p1) and CMIP6 (r1i1p1f1) models are used (models are listed in Figure S1 in Supporting Information S1). The observed and simulated outputs are analyzed from 1850 to 2005 in order to match the period of observations and CMIP models. The anomalies are calculated with respect to the climatology period from 1850 to 2005.

The temporal evolution of ENSO is expressed by the Niño3.4 index, defined as the averaged SSTA in 120°–170°W and 5°S–5°N region. The TNA index is defined as the averaged SSTA over the region 10°–70°W and 5°–25°N. The TNA events are defined as occurring when the 3-month running averaged TNA index is larger than 1.0 standard deviation and less than −1.0 standard deviation.

2.2. A Conceptual Linear Stochastic-Dynamical Model

Previous studies (Czaja, 2004; Czaja et al., 2002; Zhang et al., 2021) suggested that the interannual variations of TNA SSTA could be understood as local TNA feedbacks with the external forcing. Here, we adopt a linear stochastic-dynamical model (SDM), which is driven by ENSO forcing and stochastic forcing, for the TNA SSTA:

$$\frac{dT_A}{dt} = \alpha(t)T_A(t) + \beta(t)T_E(t) + \sigma\xi(t), \tag{1}$$

$$\frac{d\xi}{dt} = -m\xi + w(t), \tag{2}$$

where T_A and T_E are the monthly TNA index and Niño3.4 index, respectively. $\alpha(t)$ is the damping rate of TNA and $\beta(t)$ is the ENSO forcing strength. σ is the noise amplitude, $w(t)$ is the white noise term, and ξ is a normalized Gaussianly distributed red noise with a $1/m$ decay timescale. The first term on the right-side $[\alpha(t)T_A(t)]$ reflects seasonal damping by the local TNA feedbacks and the second term on the right-side $[\beta(t)T_E(t)]$ represents the remote ENSO forcing. In contrast, the model developed by Czaja (2004) only includes the seasonal dependence of ENSO forcing. In our SDM framework, both the seasonal modulation of local TNA feedbacks and ENSO forcing are considered.

The choice of model parameters $\alpha(t)$ and $\beta(t)$ are determined from the observations and CMIP models through the seasonal linear inverse model (sLIM; Section 2.3). The noise amplitude (σ) and decay rate (m) are obtained from the residual of SDM after sLIM. The SDM simulations are integrated with applied ENSO forcing from

observations and CMIP models. All SDM simulated results are from the last 20,000 years of the 21,000-year model run with a pentad (5-day) time step.

2.3. Seasonal Linear Inverse Model

To estimate the SDM parameters $\alpha(t)$, $\beta(t)$, and σ, we use a seasonal linear inverse model (sLIM) approach, which has been used to obtain the linear operator of the ENSO dynamic system with seasonal modulation (Chen & Jin, 2021). The seasonality of $\alpha(t)$ and $\beta(t)$ in Equation 1 can be considered as following approximation:

$$\alpha(t) = \alpha_0 + \alpha_1^c \cos(\omega t) + \alpha_1^s \sin(\omega t) + \alpha_2^c \cos(2\omega t) + \alpha_2^s \sin(2\omega t), \tag{3}$$

$$\beta(t) = \beta_0 + \beta_1^c \cos(\omega t) + \beta_1^s \sin(\omega t) + \beta_2^c \cos(2\omega t) + \beta_2^s \sin(2\omega t), \tag{4}$$

where $\omega = \frac{2\pi}{12\ month}$. Because the seasonality of SDM parameters beyond the semiannual cycle is so weak, we only consider the mean state (first term on the right side), annual cycle (second and third terms on the right side), and semiannual cycle (fourth and fifth terms on the right side) here. The solution of the annual modulated operators can be solved by whole matrix inversion or applying the perturbation method. The details of sLIM's procedures are described in Chen and Jin (2021). Compared to the conventional method, which estimates the annual cycle of operators based on each calendar month, the sLIM approach enables us to obtain the annual modulated operators without increasing the degrees of freedom.

2.4. Metrics of Phase-Locking

Two metrics of phase-locking are used to evaluate the features of TNA phase-locking in terms of the preferred peak month and its preference strength. As proposed by Chen and Jin (2021), the metric of phase-locking preferred peak month is defined as the calendar month of the maximum value of the peak phase histogram. The strength of phase-locking φ_s is estimated as:

$$\varphi_s = \frac{4}{3}\left(\varphi_{max} - \frac{1}{4}\right), \tag{5}$$

where φ_{max} is the sum of the 3-month greatest values of the histogram centered on its peak month. $\varphi_s = 1$ shows a complete phase-locking within a 3-month window and $\varphi_s = 0$ indicates no phase-locking.

3. Results

3.1. Features of TNA Phase-Locking

To investigate the fundamental features of TNA phase-locking, the 3-month running averaged phase histogram of SSTA peak time for observations, CMIP models, and SDM simulations are shown in Figure 1. The observed TNA events tend to peak in the boreal springtime from March to May and the probability of peaks in summer is very small (Figure 1a). In climate models, the phase histogram of the ensemble mean is similar to the observed (Figure 1e), where there is a preferred peak month in the boreal springtime, but its strength of phase-locking preference is smaller than observations and its preferred peak month shifts to late spring (from April to June). Unlike ENSO phase-locking (Chen & Jin, 2021), the climate models have a better ability to simulate TNA phase-locking in terms of the preferred calendar month and strength of this preference (Figures S1 and S2 in Supporting Information S1).

3.2. Relative Role of Damping Rate and ENSO Forcing Strength on TNA Phase-Locking

By providing the observed ENSO forcing and seasonal modulations of parameters via sLIM, the SDM simulations can well reproduce the TNA phase-locking for observations (Figure 1b) and CMIP models (Figures 1f and S3 in Supporting Information S1). Two sensitivity SDM simulations are adopted here to examine the individual influences of the seasonal modulation of SDM parameter: (a) only considering the seasonal modulation of TNA damping rate α (SDM-α; set β as annual mean), and (b) only considering the seasonal modulation of ENSO forcing strength β (SDM-β; set α as annual mean).

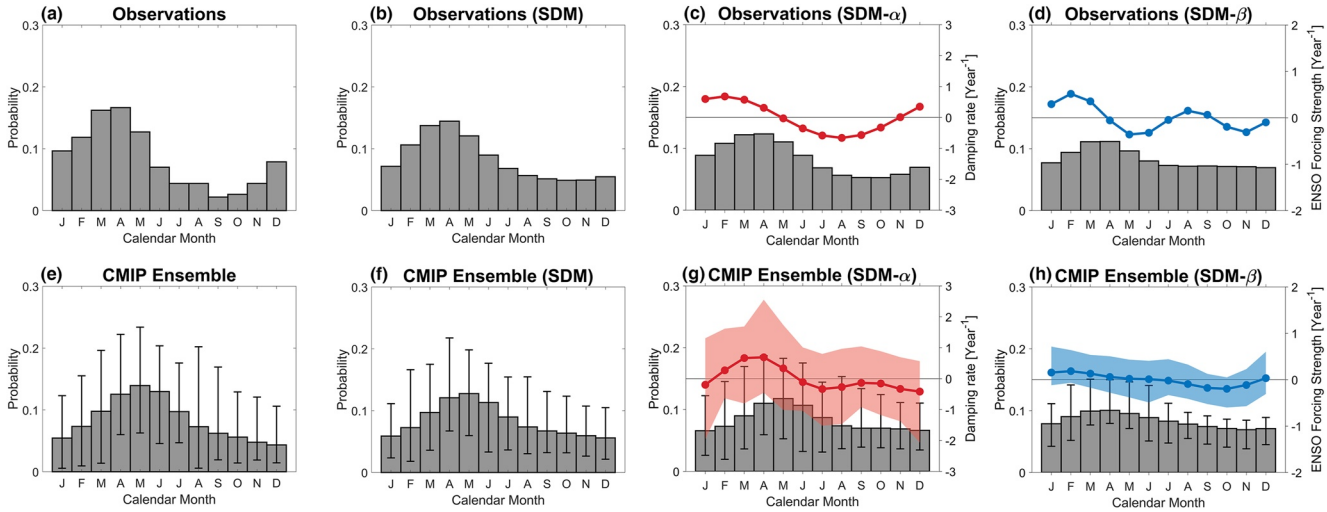

Figure 1. Peak phase histogram of TNA phase-locking (bars) for (a) observations and its (b) SDM, (c) SDM-α, and (d) SDM-β simulations. (e)–(h) Same as (a)–(d) but for ensemble mean of CMIP5 and CMIP6 models. The curves with dots are the mean-removed damping rate of TNA in (c) and (g) and mean-removed ENSO forcing strength in (d) and (h). The vertical lines and shadings in (e)–(h) indicate the minimum and maximum values of the histogram and damping rate/ENSO forcing strength, respectively.

In the observations, the role of local TNA feedbacks (SDM-α; Figure 1c) and remote ENSO forcing (SDM-β; Figure 1d) in TNA phase-locking are equivalently important, both preferring the peak of TNA variability to appear in the boreal spring with similar strength. The peak of the histogram caused by the local TNA feedbacks (ENSO forcing) appears when the seasonal modulation of α (β) transitions from positive to negative. For local TNA feedbacks, the seasonal modulation of α is dominated by the annual cycle and the semiannual component is much smaller (Figures 1c and S4a in Supporting Information S1). In contrast, for the ENSO forcing, the modulation of β has a significant semiannual cycle component, leading to relatively weaker strength for phase-locking (Figures 1d and S4b in Supporting Information S1). Because the influences of local TNA feedbacks and ENSO forcing are superimposed in boreal spring, the strength of the histogram preference in the complete SDM simulation (Figure 1b) is greater than that in SDM-α and SDM-β (Figures 1c and 1d).

For climate models, the ensemble-mean histograms of SDM-α and SDM-β also show the preferred peak in spring (Figures 1g and 1h), which is the same as observations. However, for local TNA feedbacks, the seasonal change in local TNA feedbacks α has a stronger semiannual cycle, and the transition time of α from positive to negative shifts to late spring, which leads to a delay in the preferred peak month of phase-locking (Figures 1g and S5 in Supporting Information S1). Moreover, the amplitude of seasonal modulation of ENSO forcing strength β is much weaker in most climate models (Figures 1h and S6 in Supporting Information S1), which results in a smaller strength of ENSO-related TNA phase-locking.

3.3. Parameter Dependence of TNA Phase-Locking

To investigate the sensitivity of TNA phase-locking in terms of peak month and strength, the SDM parameters (i.e., mean value of α and β, amplitude of annual cycle of α and β, amplitude of semiannual of α and β, amplitude of ENSO, and noise amplitude) are examined in this section. The range of parameters is chosen to be the models' ensemble mean plus or minus two times the standard deviation of models.

As mentioned previously, the preferred peak of the histogram occurs when the seasonal modulation of α and β transitions from positive to negative. To find out the determinants of the preferred peak month of TNA phase-locking, the largest negative derivative of α and β is chosen as the transition point. As shown in Figure 2a, the preferred peak months for local TNA feedbacks (SDM-α) and ENSO-related phase-locking (SDM-β) are mainly determined by the phases of α and β, respectively. The preferred histogram peak of SDM-α (SDM-β) appears near the largest negative derivative of the α (β) and shifts with the phase of α (β). Other parameters have little influence on the peak month of the histogram (Figure S7 in Supporting Information S1). In observations, the contributions of local TNA feedbacks and ENSO forcing on phase-locking are superimposed in the same phase, where both prefer

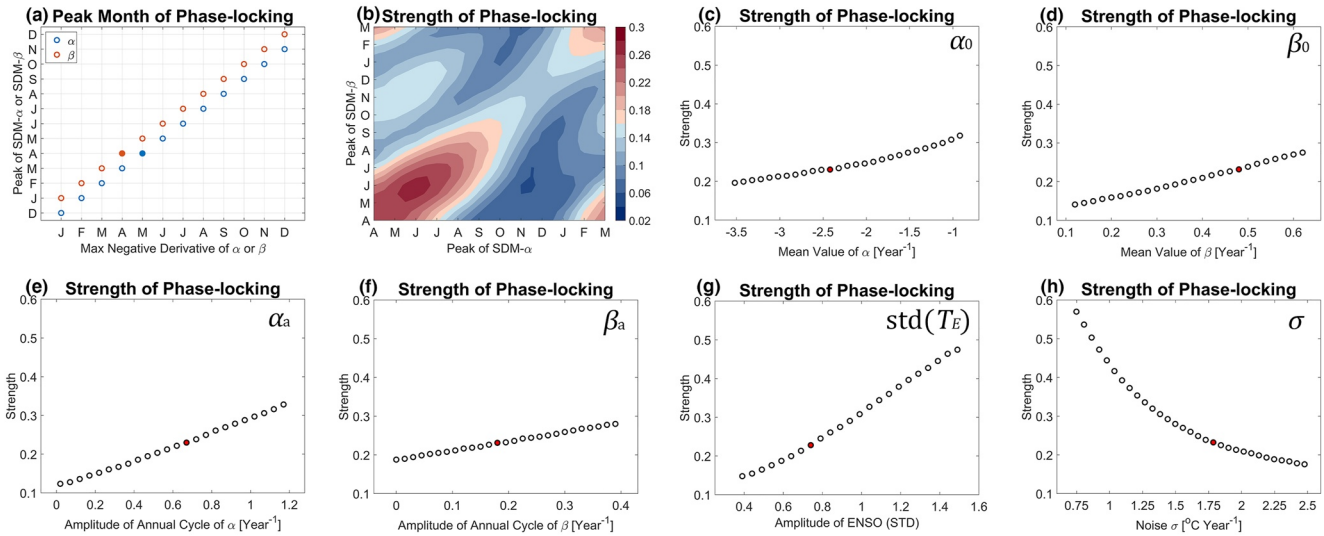

Figure 2. (a) Peak month of SDM-α and SDM-β histogram dependence on the phase of α and β. The strength of SDM TNA phase-locking dependence on (b) peak month of SDM-α and SDM-β histogram, (c) mean value of α, (d) mean value of β, (e) amplitude of annual cycle of α, (f) amplitude of annual cycle of β, (g) amplitude of ENSO (standard deviation of T_E), and (h) amplitude of noise σ. The solid red dots represent observations.

the peak of TNA variability to appear in the boreal spring. Note that there could be a phase difference between α and β, which may necessitate consideration of the combined effect of SDM-α and SDM-β on TNA phase-locking. We do not discuss the joint effect of SDM-α and SDM-β on the peak month of phase-locking here, because it is too complicated to consider both the phase difference between α and β and the relative strength of SDM-α and SDM-β on TNA phase-locking.

The phases of α and β control the preferred peak of TNA phase-locking and also impact its strength. The dependence of the strength of TNA phase-locking on the peak month of SDM-α and SDM-β histograms is shown in Figure 2b. When the preferred peak months of SDM-α and SDM-β histograms occur in the same month (along the diagonal line), their independent contributions will be superimposed and have greater strength of TNA phase-locking. If the peak months of SDM-α and SDM-β histograms differ by about 6 months, the influences of SDM-α and SDM-β will become out of phase and there will be a counteracting effect, leading to smaller TNA phase-locking strength. It is worth noting that phase-locking strength is relatively small when the peaks of both SDM-α and SDM-β histograms occur in boreal winter (November–January). This is because the winter peak phase-locking of ENSO (seasonal variance of T_E) makes the TNA inclined to peak in the boreal spring and counteract the effects of SDM-α and SDM-β, resulting in a weaker TNA phase-locking.

Next, we consider the dependence of TNA phase-locking strength on other parameters. Although the relationship between SDM parameters and phase-locking strength in climate models is weak because all of the influences of parameters are combined, we can also examine the independent influence of parameters through SDM experiment. The increase in the TNA phase-locking strength is a consequence of the increased mean value of α and β (Figures 2c and 2d), amplitude of annual cycle of α and β (Figures 2e and 2f), and amplitude of ENSO (standard deviation of T_E; Figure 2g), as well as the decreased amplitude of noise (Figure 2h). It is worth noting that the range of the strength response to changes in noise amplitude is larger than that of other parameters (Figure 2h), indicating that the amplitude of noise seems to have the greatest effect on the locking phase in the CMIP models. However, the influence of noise amplitude must be considered together with the TNA or ENSO intensity so that the amplitude of noise is not the main factor because the correlation between noise amplitude and phase-locking strength is near 0.

3.4. Control Factors of Damping Rate and ENSO Forcing Strength

In this section, the mechanism for the seasonal modulations of TNA damping rate (α) and ENSO forcing strength (β) is investigated. As suggested by previous studies, the variability of TNA SSTA is mainly dominated by the thermodynamics and ocean dynamics only play a minor role (Czaja et al., 2002; Yu et al., 2006). Here, we

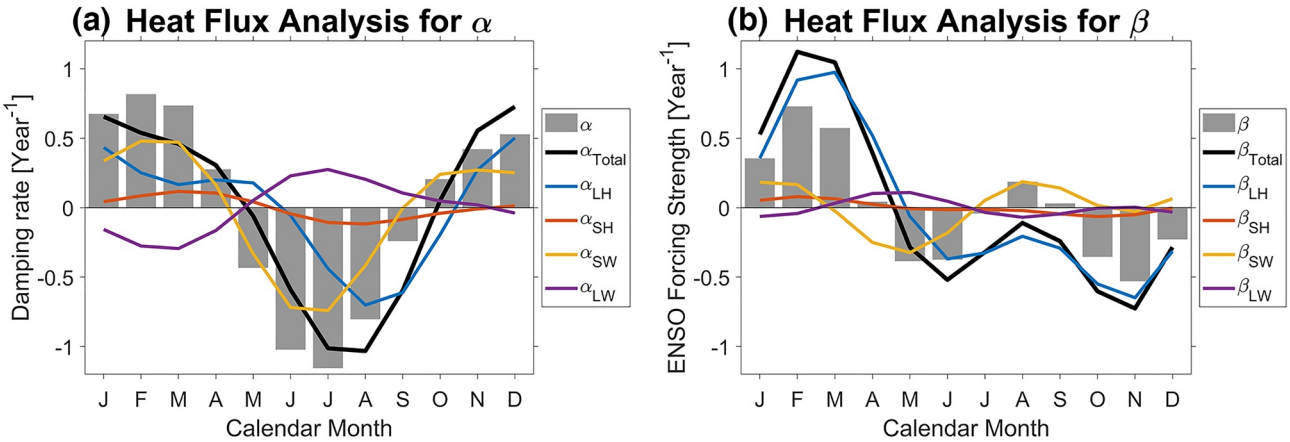

Figure 3. The contribution of surface heat flux for the seasonal modulation of (a) damping rate of TNA and (b) ENSO forcing strength. The gray bars represent the original damping rate of TNA and ENSO forcing strength. The black, blue, red, yellow, and purple curves indicate the contribution of total heat flux, latent heat flux, sensible heat flux, shortwave radiation, and longwave radiation, respectively. The mean values have been removed.

consider only the seasonal variations of surface heat flux terms (e.g., latent heat, sensible heat, shortwave radiation, and longwave radiation) as the primary control factors for the seasonal modulations of α and β. To replace the SSTA tendency term in Equation 1 by the heat flux terms:

$$\frac{Q_{Total}}{\rho C_p H} = \frac{Q_{LH} + Q_{SH} + Q_{SW} + Q_{LW}}{\rho C_p H} = (\alpha_{LH} + \alpha_{SH} + \alpha_{SW} + \alpha_{LW})T_A + (\beta_{LH} + \beta_{SH} + \beta_{SW} + \beta_{LW})T_E + \sigma\xi, \quad (6)$$

where Q_{Total}, Q_{LH}, Q_{SH}, Q_{SW}, and Q_{LW} indicate the total surface heat flux, latent heat, sensible heat, shortwave radiation, and longwave radiation, respectively, and each term of α and β on the right side is its corresponding contribution of seasonal modulation of damping rate and ENSO forcing strength. ρ, C_p, and H are the seawater density, specific heat of seawater, and mixed layer depth (set to 50 m here). Because Equation 6 is linear, we can decompose each heat flux term and estimate their contribution by sLIM as shown in Figure 3. Although there are slight differences between α (β) and α_{Total} (β_{Total}), which may be due to the neglect of seasonal change of mixed layer depth, the difference between SST and averaged mixed layer temperature, or the lack of ocean dynamics, α_{Total} and β_{Total} can almost explain the seasonal variation of α and β, confirming that thermodynamics is the main factor controlling TNA SSTA.

The seasonal modulation of the TNA damping rate is mainly attributed by the latent heat flux and shortwave radiation, and the longwave radiation tends to reduce the annual cycle amplitude of α (Figure 3a). The damping rate α is larger in the boreal winter and spring and smaller in the boreal summer and fall, leading to a maximum TNA SSTA around April. In the boreal winter and spring, the ITCZ is located near the equator causing the opposition of the anomalous and mean trade winds (Breugem et al., 2007), leading to a reduction in wind-induced latent cooling (Positive α_{LH} anomaly). During the summer and fall, the wind-induced latent cooling is stronger (Negative α_{LH} anomaly) due to the same direction of the anomalous and mean winds when the ITCZ moves northward away from the equator. For the radiation flux, when the ITCZ is closed to the equator in boreal winter and spring, the radiative processes over the TNA region are dominated by feedback between low-level stratus cloud and SST (Okumura et al., 2001; Tanimoto & Xie, 2002). A positive SSTA will reduce the amount of stratus clouds, enhance the incoming shortwave radiation (Positive α_{SW} anomaly) and reduce the downward longwave radiation (negative α_{LW} anomaly). As the ITCZ moves northward into TNA region during boreal summer and fall, the radiative feedback is controlled by the deep cumulonimbus clouds (Okumura et al., 2001; Tanimoto & Xie, 2002). An increase in cumulonimbus cloudiness due to positive SSTA will reduce incoming shortwave radiation (negative α_{SW} anomaly) and increase downward longwave radiation (positive α_{LW} anomaly).

In contrast, the seasonal modulation of ENSO forcing strength is primarily contributed by the latent heat flux only (Figure 3b), which is consistent with previous studies: the evolution of TNA SSTA associated with ENSO is controlled by the latent heat flux, caused by the ENSO-induced change of wind anomalies over TNA region

(Czaja, 2004; Jiang & Li, 2019). There is an efficient modulation of the strength of the trade wind during boreal spring and weak changes in surface wind anomalies in boreal summer and fall over the TNA region. This seasonality in the remote ENSO teleconnection could be due to the response of seasonal cycle of convection over the TNA to the ENSO-induced SSTA of the troposphere (Chiang & Sobel, 2002), or the seasonal modulation of the ENSO-forced Pacific North American pattern (Nobre & Shukla, 1997).

3.5. Contribution of ENSO on TNA Phase-Locking

As mentioned previously, the contribution of ENSO on TNA phase-locking is weak in most climate models. To investigate the key factors of ENSO influence on TNA phase-locking in climate models, the scatterplot of the strength of ENSO-related TNA phase-locking (SDM-β) and maximum lead-lag correlation between ENSO and TNA is shown in Figure 4. In most climate models, their maximum correlation appears when ENSO leads TNA about 3–6 months, which is consistent with observations (Figure S8 in Supporting Information S1). It is not surprising that models with higher correlations have greater ENSO-related TNA phase-locking strengths (Figure 4a). Most models have a smaller contribution of ENSO on TNA phase-locking and poorer relationship between ENSO and TNA. Further, we found that this relationship in climate models is highly correlated with the ENSO-induced wind speed response over TNA region (Figure 4b).

Because the ENSO-related wind variations in the TNA region are primarily caused by the extratropical forcing via the Pacific North American pattern (PNA; Jiang & Li, 2019), the regressions of 850 hPa geopotential height and wind onto normalized Niño3.4 are used to investigate the ENSO teleconnection patterns in climate models with different correlations between ENSO and TNA. In observations and model ensemble mean (Figures 4e and 4f), the PNA low-level pattern exists as a significant low-pressure system over the southeastern United States, corresponding southwesterly anomalies along the low-pressure in TNA region. The ENSO-associated southwesterly anomalies weaken the northeasterly trade winds and reduce the wind speed over TNA region, leading to the warming of the TNA SSTA (Alexander & Scott, 2002; Enfield & Mayer, 1997; Giannini et al., 2000; Klein et al., 1999).

Next, we define the models with correlation greater than 1.0 standard deviation (less than −1.0 standard deviation) from an ensemble mean as a high correlation group (low correlation group). For the high correlation group, there is a more significant PNA low-level pattern, which means that the low-pressure system over the southeastern United States can extend eastward into the TNA region with greater strength (Figures 4g and S9 in Supporting Information S1). In contrast, for models in the low correlation group, the low-pressure system may not reach the TNA region or the intensity is much weaker (Figures 4h and S9 in Supporting Information S1). For the models that have higher correlation between ENSO and TNA, their seasonal mean of ENSO forcing strength (β) and amplitude of ENSO (standard deviation of T_E) will be larger (Figures 4c and 4d), leading to a larger contribution of ENSO on TNA phase-locking.

4. Summary and Discussion

In this study, a conceptual linear SDM is developed to investigate the TNA phase-locking. By considering the seasonal modulation of local TNA feedbacks and remote ENSO forcing, SDM can well reproduce the TNA phase-locking both in observations and CMIP models. In the observations, the role of local TNA feedbacks and ENSO forcing are equally important in TNA phase-locking, with both having the peaks of TNA variability to occur in the boreal spring. The seasonal modulation of TNA damping rate (α) and ENSO forcing strength (β) are mainly controlled by thermodynamic processes, where TNA damping rate is caused by latent heat flux, shortwave, and longwave radiation, but ENSO forcing strength is mainly controlled by latent heat flux. In most climate models, TNA has a phase-lock in the late boreal spring and both local TNA feedbacks and ENSO forcing prefer to have the peaks of TNA SSTA appear in the springtime. However, the contribution of remote ENSO forcing on TNA phase-locking is weak in most models. The TNA phase-locking strength associated with ENSO is highly correlated with the relationship between ENSO and TNA, which is mainly determined by the amplitude of ENSO and its low-level teleconnection patterns. A stronger ENSO amplitude with a more eastward extending remote teleconnection pattern would have a higher impact on TNA and lead to a greater contribution of ENSO to TNA phase-locking.

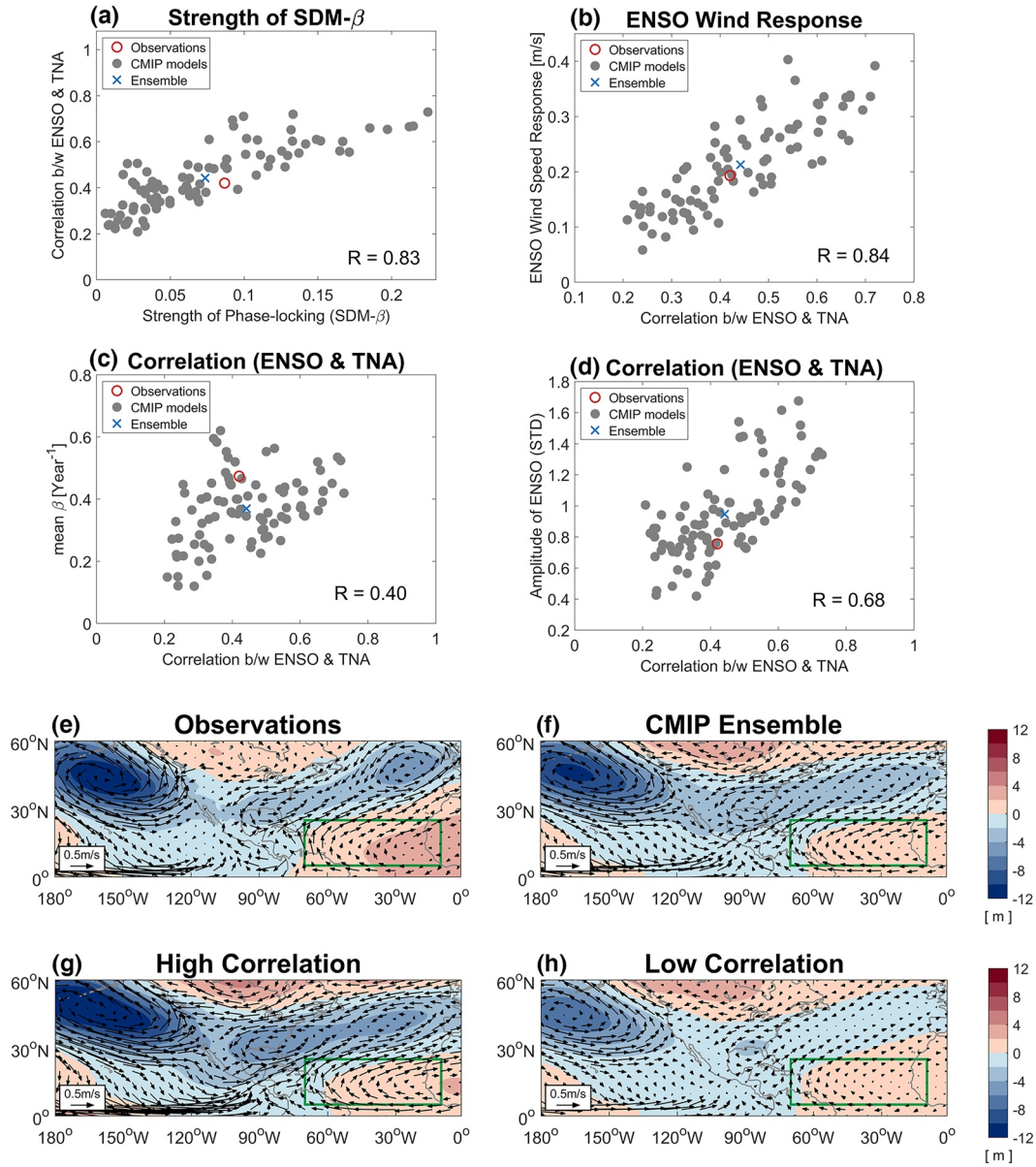

Figure 4. (a) Scatterplot of the strength of ENSO-related TNA phase-locking (SDM-β) and maximum correlation between ENSO and TNA. The scatterplot of maximum correlation between ENSO and TNA and (b) regression of wind speed onto normalized Niño3.4 over TNA region, (c) mean value of β, and (d) amplitude of ENSO. The red circle and blue cross indicate the observations and ensemble mean of CMIP models, respectively. Regression of 850 hPa geopotential height (shading) and wind (vectors) onto normalized Niño3.4 for (e) observations, (f) ensemble mean, (g) high, and (h) low correlation group.

These results provide a novel approach to evaluate the relative contributions of local TNA feedbacks and remote ENSO forcing to TNA phase-locking. Although the performance of TNA phase-locking is better than that of ENSO phase-locking in CMIP models, it is unclear if the dynamics of TNA phase-locking in these models are correct and why some models have incorrect TNA phase-locking. The control factors of damping rate and ENSO forcing strength in climate models need to be further analyzed. Further, the teleconnection strength and pattern of Eastern-Pacific (EP) and Central-Pacific (CP) ENSO and their impact on TNA are quite different (Amaya & Foltz, 2014; Taschetto et al., 2016). The EP El Niño can induce significant warming of the TNA SSTA after its peak, but CP El Niño fails to generate significant warming in the TNA region. The difference in the contribution of EP and CP ENSO to TNA phase-locking needs to be further examined.

Data Availability Statement

All data sets used in this research can be accessed via the following websites: HadISST at https://www.metoffice.gov.uk/hadobs/hadisst/data/download.html; ERA5 at https://cds.climate.copernicus.eu/cdsapp#!/dataset/reanalysis-era5-pressure-levels-monthly-means?tab=form; https://cds.climate.copernicus.eu/cdsapp#!/dataset/reanalysis-era5-pressure-levels-monthly-means-preliminary-back-extension?tab=form; https://cds.climate.copernicus.eu/cdsapp#!/dataset/reanalysis-era5-single-levels-monthly-means?tab=form; and https://cds.climate.copernicus.eu/cdsapp#!/dataset/reanalysis-era5-single-levels-monthly-means-preliminary-back-extension?tab=form; CMIP5 at https://esgf-node.llnl.gov/search/cmip5/; CMIP6 at https://esgf-node.llnl.gov/search/cmip6/.

Acknowledgments
The authors thank all colleagues and students who contributed to this study. Fei-Fei Jin and Han-Ching Chen were supported by the U.S. NSF Grant AGS-1813611 and the Department of Energy Grant DE-SC0005110.

References

Alexander, M., & Scott, J. (2002). The influence of ENSO on air-sea interaction in the Atlantic. *Geophysical Research Letters*, *29*(14), 46-1–46-4. https://doi.org/10.1029/2001GL014347

Amaya, D. J., & Foltz, G. R. (2014). Impacts of canonical and Modoki El Niño on tropical Atlantic SST. *Journal of Geophysical Research: Oceans*, *119*(2), 777–789. https://doi.org/10.1002/2013JC009476

Breugem, W. P., Hazeleger, W., & Haarsma, R. J. (2007). Mechanisms of northern tropical Atlantic variability and response to CO_2 doubling. *Journal of Climate*, *20*(11), 2691–2705. https://doi.org/10.1175/JCLI4137.1

Chang, P., Saravanan, R., Ji, L., & Hegerl, G. C. (2000). The effect of local sea surface temperatures on atmospheric circulation over the tropical Atlantic sector. *Journal of Climate*, *13*(13), 2195–2216. https://doi.org/10.1175/1520-0442(2000)013<2195:TEOLSS>2.0.CO;2

Chen, H.-C., & Jin, F.-F. (2021). Simulations of ENSO phase-locking in CMIP5 and CMIP6. *Journal of Climate*, *1*, 1–42. https://doi.org/10.1175/jcli-d-20-0874.1

Chiang, J. C. H., Kushnir, Y., & Giannini, A. (2002). Deconstructing Atlantic intertropical convergence zone variability: Influence of the local cross-equatorial sea surface temperature gradient and remote forcing from the Eastern Equatorial Pacific. *Journal of Geophysical Research: Atmospheres*, *107*(1–2). https://doi.org/10.1029/2000jd000307

Chiang, J. C. H., & Sobel, A. H. (2002). Tropical tropospheric temperature variations caused by ENSO and their influence on the remote tropical climate. *Journal of Climate*, *15*(18), 2616–2631. https://doi.org/10.1175/1520-0442(2002)015<2616:TTTVCB>2.0.CO;2

Czaja, A. (2004). Why is north tropical Atlantic SST variability stronger in boreal spring? *Journal of Climate*, *17*(15), 3017–3025. https://doi.org/10.1175/1520-0442(2004)017<3017:WINTAS>2.0.CO;2

Czaja, A., van der Vaart, P., & Marshall, J. (2002). A diagnostic study of the role of remote forcing in tropical Atlantic variability. *Journal of Climate*, *15*(22), 3280–3290. https://doi.org/10.1175/1520-0442(2002)015<3280:ADSOTR>2.0.CO;2

Enfield, D. B., & Mayer, D. A. (1997). Tropical Atlantic sea surface temperature variability and its relation to El Niño-Southern Oscillation. *Journal of Geophysical Research: Oceans*, *102*(1), 929–945. https://doi.org/10.1029/96jc03296

Eyring, V., Bony, S., Meehl, G. A., Senior, C. A., Stevens, B., Stouffer, R. J., & Taylor, K. E. (2016). Overview of the Coupled Model Intercomparison Project Phase 6 (CMIP6) experimental design and organization. *Geoscientific Model Development*, *9*(5), 1937–1958. https://doi.org/10.5194/gmd-9-1937-2016

García-Serrano, J., Cassou, C., Douville, H., Giannini, A., & Doblas-Reyes, F. J. (2017). Revisiting the ENSO teleconnection to the tropical North Atlantic. *Journal of Climate*, *30*(17), 6945–6957. https://doi.org/10.1175/JCLI-D-16-0641.1

Giannini, A., Kushnir, Y., & Cane, M. A. (2000). Interannual variability of Caribbean rainfall, ENSO, and the Atlantic Ocean. *Journal of Climate*, *13*(2), 297–311. https://doi.org/10.1175/1520-0442(2000)013<0297:IVOCRE>2.0.CO;2

Hersbach, H., Bell, B., Berrisford, P., Hirahara, S., Horányi, A., Muñoz-Sabater, J., et al. (2020). The ERA5 global reanalysis. *Quarterly Journal of the Royal Meteorological Society*, *146*(730), 1999–2049. https://doi.org/10.1002/qj.3803

Jiang, L., & Li, T. (2019). Relative roles of El Niño-induced extratropical and tropical forcing in generating Tropical North Atlantic (TNA) SST anomaly. *Climate Dynamics*, *53*(7–8), 3791–3804. https://doi.org/10.1007/s00382-019-04748-7

Klein, S. A., Soden, B. J., & Lau, N. C. (1999). Remote sea surface temperature variations during ENSO: Evidence for a tropical atmospheric bridge. *Journal of Climate*, *12*(4), 917–932. https://doi.org/10.1175/1520-0442(1999)012<0917:RSSTVD>2.0.CO;2

Nobre, P., & Shukla, J. (1997). Variations of sea surface temperature, wind stress, and rainfall over the tropical Atlantic and South America. *Oceanographic Literature Review*, *5*(44), 437.

Okumura, Y., Xie, S.-P., Numaguti, A., & Tanimoto, Y. (2001). Tropical Atlantic air-sea interaction and its influence on the NAO. *Geophysical Research Letters*, *28*, 1507–1510. https://doi.org/10.1029/2000gl012565

Rayner, N. A., Parker, D. E., Horton, E. B., Folland, C. K., Alexander, L., Rowell, D. P., et al. (2003). Global analyses of sea surface temperature, sea ice, and night marine air temperature since the late nineteenth century. *Journal of Geophysical Research: Atmospheres*, *108*(D14). https://doi.org/10.1029/2002jd002670

Saravanan, R., & Chang, P. (2000). Interaction between tropical Atlantic variability and El Nino-Southern Oscillation. *Journal of Climate*, *13*(13), 2177–2194. https://doi.org/10.1175/1520-0442(2000)013<2177:IBTAVA>2.0.CO;2

Tanimoto, Y., & Xie, S.-P. (2002). Inter-hemispheric decadal variations in SST, surface wind, heat flux and cloud cover over the Atlantic Ocean. *Journal of the Meteorological Society of Japan*, *80*, 1199–1219. https://doi.org/10.2151/jmsj.80.1199

Taschetto, A. S., Rodrigues, R. R., Meehl, G. A., McGregor, S., & England, M. H. (2016). How sensitive are the Pacific–tropical North Atlantic teleconnections to the position and intensity of El Niño-related warming? *Climate Dynamics*, *46*(5–6), 1841–1860. https://doi.org/10.1007/s00382-015-2679-x

Taylor, K. E., Stouffer, R. J., & Meehl, G. A. (2012). An overview of CMIP5 and the experiment design. *Bulletin of the American Meteorological Society*, *93*(4), 485–498. https://doi.org/10.1175/BAMS-D-11-00094.1

Yu, L., Jin, X., & Weller, R. A. (2006). Role of net surface heat flux in seasonal variations of sea surface temperature in the tropical Atlantic Ocean. *Journal of Climate*, *19*(23), 6153–6169. https://doi.org/10.1175/JCLI3970.1

Zhang, W., Jiang, F., Stuecker, M. F., Jin, F.-F., & Timmermann, A. (2021). Spurious North Tropical Atlantic precursors to El Niño. *Nature Communications*, *12*(1). https://doi.org/10.1038/s41467-021-23411-6